Soft Matter

PAPER

Check for updates

Cite this: *Soft Matter*, 2018, **14**, 2835

Received 19th February 2018,
Accepted 22nd March 2018

DOI: 10.1039/c8sm00342d

rsc.li/soft-matter-journal

First-order wedge wetting revisited

C. Rascón, [a] J. Pausch [b] and A. O. Parry [b]

We consider a fluid adsorbed in a wedge made from walls that exhibit a first-order wetting transition and revisit the argument as to why and how the pre-filling and pre-wetting coexistence lines merge when the opening angle is increased approaching the planar geometry. We clarify the nature of the possible surface phase diagrams, pointing out the connection with complete pre-wetting, and show that the merging of the coexistence lines lead to new interfacial transitions. These occur along the side walls and are associated with the unbinding of the thin-thick interface, rather than the liquid–gas interface (meniscus), from the wedge apex. When fluctuation effects, together with the influence of dispersion forces are included, these transitions display strong non-universal critical singularities that depend on the opening angle itself. Similar phenomena are also shown to occur for adsorption near an apex tip.

1 Introduction

The equilibrium phases of a fluid in a restricted geometry often depend crucially on the wetting properties of the confining walls.[1] This means that rather rich phase diagrams can be produced from the interplay between wetting and new phase transitions induced by even simple substrate shapes. In this paper, we illustrate this by revisiting the problem of fluid adsorption in a wedge, for systems exhibiting first-order wetting transitions.[2–5] Here, the richness of the phase diagram arises because, away from bulk two-phase coexistence, the wedge-fluid interface exhibits not only a line of pre-wetting transitions but also a line of pre-filling transitions. In general, these lines are separate; however, for sufficiently shallow wedges they must merge at two points before eventually becoming identical when the wedge is opened to recover the planar geometry, as first shown by Rejmer, Napiorkowski and Dietrich.[2] Here, we clarify the nature of the phase diagram and stress the connection with continuous or complete pre-wetting transitions which has not been understood previously.[6,7] In particular, we show that the merging of the pre-filling and pre-wetting lines leads necessarily to additional first-order and continuous interfacial unbinding transitions occurring along the side walls of the wedge.

We begin by determining the phase diagram for fluid adsorption in a shallow wedge at mean-field level, using a very simple interfacial model of wetting and filling. Here, the merging of the pre-filling and pre-wetting lines can be demonstrated analytically (following ref. 2 and 3) using graphical techniques similar to those used in the original Cahn square-gradient theory of wetting.[8,9] Then, we go beyond mean-field analysis, stressing what transitions remain and what transitions are rounded when interfacial fluctuation effects are included. In particular, for fluids with long-ranged dispersion-like forces, we show that the new unbinding transitions occurring along the side walls may be characterised by highly non-universal critical singularities. These depend sensitively on the value of the opening angle itself and are related to the fluctuation theory of 2D wetting with marginal interactions.[10] Similar phenomena are also shown to occur for adsorption near an apex tip, where the role of pre-filling is replaced by unbending transitions.[11]

2 Wetting and pre-wetting, filling and pre-filling

2.1 Wetting and pre-wetting at a planar wall

Consider a planar wall in contact with a vapour at sub-critical temperature T and pressure p (or chemical potential μ) close to the bulk two-phase coexistence curve $p_{\rm sat}(T)$. We suppose that, along the bulk coexistence curve, the wall–vapour interface exhibits a wetting transition at temperature $T_{\rm w}$ at which the contact angle $\theta(T)$ vanishes – for comprehensive reviews see for example.[12–15] Further, we suppose that the wetting transition is first-order in character so that the adsorption of liquid changes discontinuously from a microscopic to a macroscopic value at $T_{\rm w}$. In three dimensions, first-order wetting is also associated with a line of pre-wetting transitions, extending tangentially away from bulk coexistence in the $(T,\Delta p = p_{\rm sat} - p)$ plane. Along this line, two phases with different microscopic adsorptions, referred to as "thin" and "thick", are in coexistence. The pre-wetting line ends at a pre-wetting critical point, where the thin and thick phases are no longer distinguishable. A simple

[a] GISC, Department of Mathematics, Universidad Carlos III Madrid, Madrid, Spain. E-mail: carlos.rascon@uc3m.es
[b] Department of Mathematics, Imperial College London, London SW7 2AZ, UK

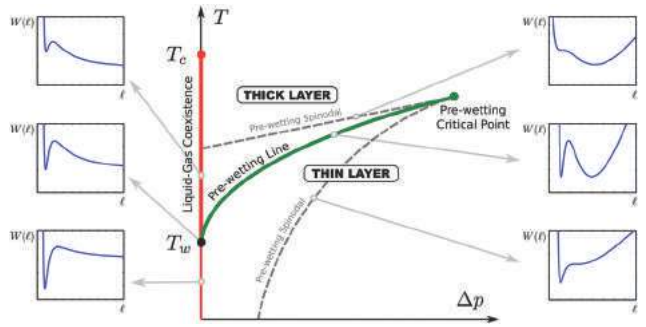

Fig. 1 Phase diagram for first-order wetting showing the wetting temperature T_w and pre-wetting line (green) ending at the pre-wetting critical point. Dashed lines refer to mean-field spinodals. Liquid–gas coexistence corresponds to $\Delta p = 0$ (red line). The wall–vapour interface is completely wet by liquid for $T \geq T_w$ (thick part of the red line) up to the bulk critical temperature T_c. The qualitative shape of the binding potential $W(\ell)$ below, at, and above the wetting transition, along the pre-wetting line and at the spinodals is also shown in the insets.

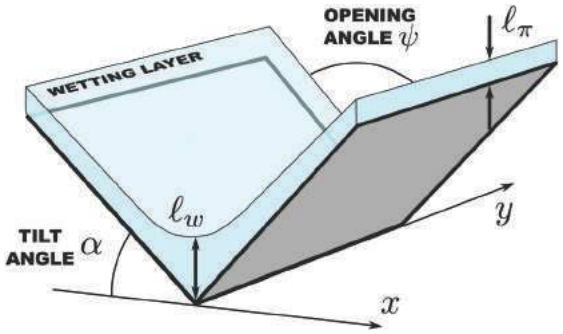

Fig. 2 Schematic illustration of an interfacial configuration in a shallow wedge showing the mid-point height ℓ_w and planar wetting film thickness ℓ_π. Translational invariance is assumed along the y-axis of the wedge.

way of modelling first-order wetting and pre-wetting transitions at mean-field level is based on the minimization of a binding potential $W(\ell)$. This potential corresponds to the excess free-energy (per unit area) of a liquid wetting layer of uniform thickness ℓ. The precise form of $W(\ell)$ depends on the specific wall–fluid and fluid–fluid intermolecular forces, but for first-order wetting and pre-wetting it must necessarily exhibit a barrier between local and global minima, representing the thin and thick wetting layers. The phase diagram for first-order wetting is shown in Fig. 1, which also illustrates the qualitative features of the binding potential near wetting along the pre-wetting line and near the spinodals.

2.2 Filling and pre-filling near a wedge

Now consider that the wall is sculpted to the shape of a wedge with opening angle ψ. We suppose that the wedge is translationally invariant along the y axis so that the height of the wall above the $z = 0$ plane (say) is described by the function $z_w = |x| \tan\alpha$. We will refer to $\alpha = (\pi - \psi)/2$ as the tilt angle of the wedge. At two phase coexistence, a wedge–vapour interface necessarily undergoes a filling transition at a temperature $T_f < T_w$ satisfying the thermodynamic condition[16–18]

$$\theta(T_f) = \alpha \tag{1}$$

so that for $T > T_f$ the wedge is completely filled with liquid. For wedges made from walls showing strong first-order wetting transitions (*i.e.* with a prominent activation barrier in $W(\ell)$), the filling transition is also anticipated to be first-order.[2,3] Thus, the change from a microscopic to a macroscopic adsorption of liquid occurring at T_f is discontinuous. By analogy with first-order wetting, we also expect that first-order filling is associated with a line of pre-filling transitions extending tangentially away from T_f in the $(T,\Delta p)$ plane and terminating at a pre-filling critical point. This represents the line of coexistence between adsorptions of small and larger amounts of liquid near the wedge bottom for $p < p_{sat}$. Beyond mean-field level, pre-filling transitions are rounded by fluctuations, although this rounding is very small close to p_{sat}; we will return to this at the end of our paper.

At mean-field level, filling and pre-filling transitions can be easily studied using a simple free-energy functional incorporating the surface tension σ and the binding potential. For shallow wedges, on which our study focuses, the free-energy per unit length along the y-axis can be written as[3]

$$F[\ell] = \int \mathrm{d}x \left(\frac{\sigma}{2} \left(\frac{\mathrm{d}\ell}{\mathrm{d}x} \right)^2 + W(\ell - \alpha|x|) \right) \tag{2}$$

where $\ell(x)$ represents the local height of the interface above the plane, and we have assumed translational invariance along the wedge. A schematic section of the wedge geometry is shown in Fig. 2. The first term in (2) represents the free-energy cost of increasing the area of the interface, induced by the geometry, while the final term allows for the intermolecular forces, assuming that these can be modelled using the same binding potential constructed for a planar wall. This local functional is not appropriate for studying filling in acute wedges but for most purposes is legitimate, provided the wedge is shallow and we can approximate $\tan\alpha \approx \alpha$. The model (2) was studied in ref. 2 and 3, where the authors showed how the filling phase diagram can be understood using simple graphical methods. We repeat this here, since the finer details and their implications for the phase diagram at mean-field level and beyond were not fully appreciated.

Minimization of (2) leads to the Euler–Lagrange equation for the equilibrium interfacial configuration

$$\sigma \ddot{\ell} = W'(\ell - \alpha|x|) \tag{3}$$

where we have abbreviated $\ddot{\ell} \equiv \mathrm{d}^2\ell/\mathrm{d}x^2$, while the prime denotes differentiation w.r.t. ℓ. This must be solved subject to the boundary conditions $\ddot{\ell}(0) = 0$ and that $\ell - \alpha|x| \to \ell_\pi$ as $|x| \to \infty$, where ℓ_π denotes the equilibrium wetting layer thickness at a planar wall, *i.e.* corresponding to the global minimum of $W(\ell)$. The first integral of (3) determines the relative interfacial height $\eta(x) \equiv \ell(x) - \alpha|x|$. For $x < 0$, this satisfies

$$\dot{\eta} = \sqrt{\frac{2\Delta W(\eta)}{\sigma}} \tag{4}$$

This journal is © The Royal Society of Chemistry 2018

and similarly for $x > 0$, but with a change of sign by symmetry. Here, $\Delta W(\ell) \equiv W(\ell) - W(\ell_\pi)$ is a shifted binding potential which has a global minimum at ℓ_π so that $\Delta W(\ell_\pi) = 0$. Substituting (4) into (2), and subtracting unimportant constant terms, it follows that the excess wedge free-energy (per unit length) of an equilibrium configuration is given by

$$\tau = 2\sigma \int_{\ell_\pi}^{\ell_w} \mathrm{d}\ell \left(\sqrt{\frac{2\Delta W(\ell)}{\sigma}} - \alpha \right) \tag{5}$$

where $\ell_w \equiv \ell(0)$ is the mid-point interfacial height, which is itself obtained *via* the very simple equation

$$\alpha = \sqrt{\frac{2\Delta W(\ell_w)}{\sigma}} \tag{6}$$

These equations have a simple interpretation whereby the intersection of a horizontal line at height α with the graph of $\sqrt{2\Delta W(\ell)/\sigma}$ determines the value of ℓ_w and, hence, the phase portrait $(\eta, \dot{\eta})$ of the equilibrium profile. Consider, for example, the situation at bulk coexistence and $T < T_w$ (see Fig. 3a), for which the graph $\sqrt{2\Delta W(\ell)/\sigma}$ is zero at ℓ_π, has a potential barrier and a horizontal asymptote at height θ. The latter follows from Young's equation $W(\ell_\pi) = \sigma(\cos\theta - 1)$, which in the present small angle approximation is consistently written $W(\ell_\pi) = -\sigma\theta^2/2$. It follows that the wedge geometry must exhibit a filling transition at the anticipated thermodynamic boundary $\theta = \alpha$ since there are then microscopic and macroscopic solutions for the mid-point height ℓ_w.

A similar graphical analysis determines the pre-filling line off bulk coexistence. In this case, the expression (5) for the free-energy leads to a simple equal areas construction for the coexistence of distinct interfacial configurations with different values of the mid-point thickness $\ell_w^{(-)}$ and $\ell_w^{(+)}$ which have the same equilibrium free-energy τ (see Fig. 3b). The pre-filling line necessarily joins the bulk coexistence line $p_{sat}(T)$ tangentially at T_f because the difference in the adsorptions of the coexisting phases becomes macroscopic in this limit.[13,14] Similarly, the present graphical construction determines that the pre-filling line terminates at a point which must lie on the line of spinodals associated with the pre-wetting line, *i.e.* when the binding potential $W(\ell)$ loses the metastable minimum corresponding to the thicker film (see Fig. 3c). This means that the temperature of the pre-filling critical point lies necessarily below that of the pre-wetting critical point.

3 Pre-filling *versus* pre-wetting near a wedge

In order to model first-order wetting in systems with long-ranged dispersion-like forces, we may use the general potential[14,19]

$$W(\ell) = \frac{A}{\ell^2} - \frac{B}{\ell^3} + \frac{C}{\ell^4} + \Delta p \ell \tag{7}$$

where $A(T) > 0$ is the Hamaker constant and, similarly, $B, C > 0$ are constants which may be chosen to alter the depth of the potential and height of the barrier. The potential $W(\ell)$ together with the values of the constants A, B, C may be derived from more microscopic density functional models using, for example, a sharp-kink or soft-kink approximation for the density profile.[19] As expression (7) leads to $A(T_w) = B^2/4C$, and in order to represent the results in terms of the temperature (rather than $A(T)$), we assume without loss of generality that $A(T) - A(T_w) \propto T - T_w$. For later purposes, we note that the Hamaker constant may always be written $A = A_{wf} - A_{ff}$ where $A_{wf} > 0$ and $A_{ff} > 0$ are contributions which are directly proportional to the strength of the wall–fluid and fluid–fluid intermolecular potentials, respectively.

We have determined the phase diagram for this class of potentials and find that they fall into two categories depending on whether the tilt angle is smaller or larger than a certain critical value α^*. In both cases, the filling and wetting transitions are first-order but the nature of the pre-wetting and pre-filling lines, and associated phase transitions, are quite different (see Fig. 4a).

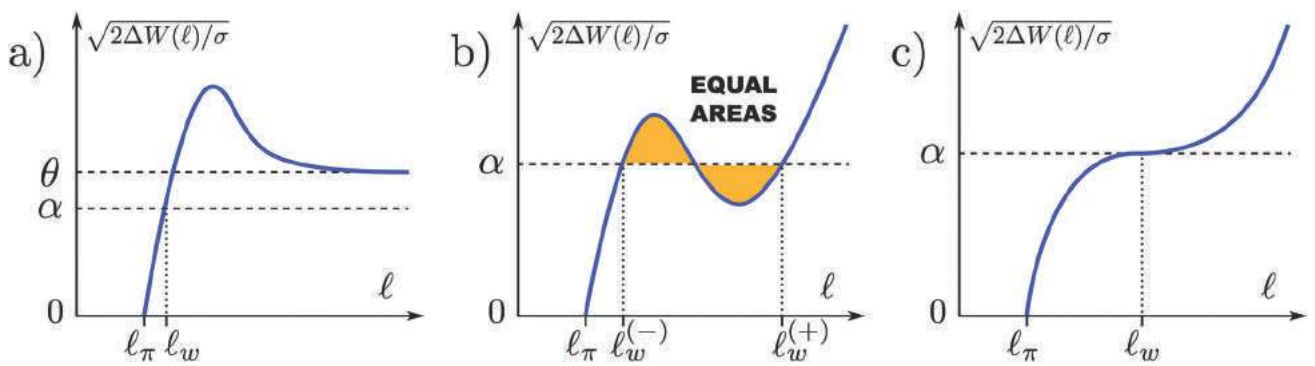

Fig. 3 Graphical construction for the equilibrium mid-point height ℓ_w at different points of the phase diagram: (a) for a first-order filling transition at bulk coexistence. The intersection of $\sqrt{2\Delta W(\ell)/\sigma}$ with the horizontal line at height α determines ℓ_w. For $\alpha < \theta$, only one solution exists. For $\theta = \alpha$, corresponding to the filling transition phase boundary, microscopic and macroscopic adsorptions of liquid in the wedge coexist. (b) At a point along the pre-filling line for which phases with different filling heights $\ell_w^{(-)}$ and $\ell_w^{(+)}$ coexist. The orange regions have equal areas. (c) At a pre-filling critical point. An equal areas construction is no longer possible when the function $\Delta W(\ell)$ has a point of inflection implying that the pre-filling point lies necessarily on the line of spinodals for the pre-wetting transition. These graphical constructions can also be interpreted as phase-portraits $(\eta, \dot{\eta})$.

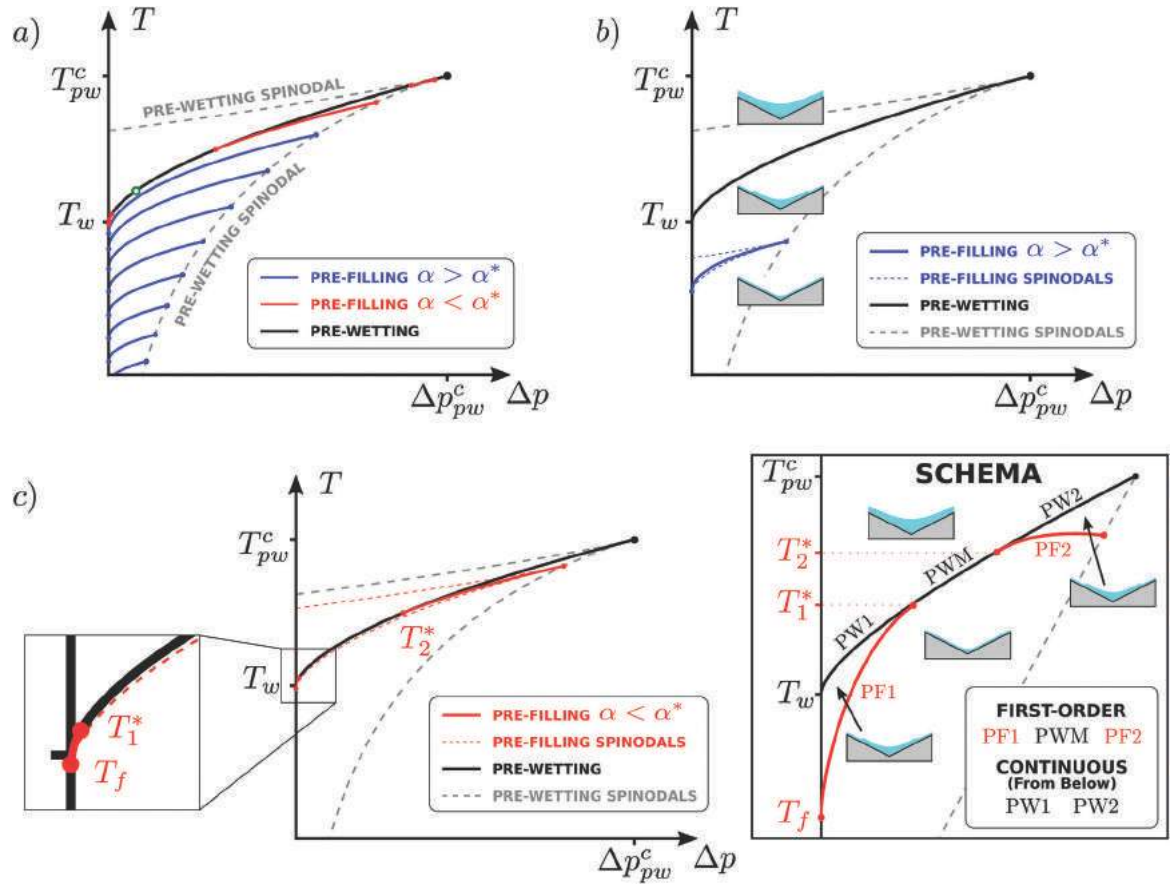

Fig. 4 Surface phase diagram for first-order wedge-filling transitions computed numerically using the binding potential (7): (a) pre-filling lines for different values of the tilting angle α. Each of these lines finishes at a critical point that lies at the (lower) pre-wetting spinodal line. As α decreases, the pre-filling line moves towards the pre-wetting line (in black). For $\alpha > \alpha^*$ (blue lines), they do not touch the pre-wetting line. In the limiting case $\alpha = \alpha^*$, the pre-filling line touches the pre-wetting line tangentially at a single point, represented by the green circle. For $\alpha < \alpha^*$ (red lines), the pre-filling lines consist of two parts that touch the pre-wetting line at two points, one at each side of the green point. (b) For $\alpha \approx 4.2\alpha^*$, the surface phase diagram shows separate pre-filling and pre-wetting lines which do not intersect. The lower pre-filling spinodal follows closely the pre-filling line and merges with it at both ends, in sharp contrast with the lower pre-wetting spinodal, which only merges with the pre-wetting line at its critical point. Three schematic configurations of the interface at different points of the diagram are also shown. The phase diagram shows two transitions: first-order pre-filling (blue line) and continuous complete pre-wetting (black line). (c) For $\alpha \approx 0.80\alpha^*$, the pre-filling lines (solid red) meet the pre-wetting line (solid black) tangentially at temperatures T_1^* and T_2^*. Note that the two parts of the pre-filling lines have common upper and lower spinodal lines (dashed red). The splitting of the pre-filling and pre-wetting line is shown schematically. There is no metastable continuation of the pre-filling line that joins the two points at T_1^* and T_2^*.

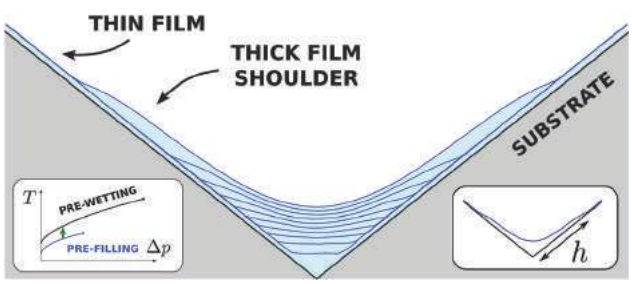

Fig. 5 Interfacial profiles in the approach to a complete pre-wetting transition as the pre-wetting line is approached from below (green arrow in inset). On approaching the pre-wetting line, the profile develops a large shoulder of the thicker pre-wetting film which intrudes between the wedge apex and the thin pre-wetting layer. The length h of this complete pre-wetting layer diverges continuously as the pre-wetting line is approached.

3.1 Case $\alpha > \alpha^*$

If the tilt angle is larger than the critical value, then the pre-filling and pre-wetting lines do not intersect, as illustrated in Fig. 4b. As described above, distinct profiles with different mid-point interfacial heights ℓ_w, but identical wetting layer thickness (far from the bottom) ℓ_π, coexist along the pre-filling line. However, something very different occurs as we approach the pre-wetting line from below, by increasing the pressure (decreasing Δp) along an isotherm, say. In this case, there is no substantive change in the mid-point height ℓ_w. Rather, the interfacial profile develops a long shoulder of the metastable thicker pre-wetting phase along each wall. As the pre-wetting line is approached, the length h of this shoulder increases continuously and becomes macroscopic at the pre-wetting line (see Fig. 5). Thus, when approached from below, the pre-wetting line serves to induce a line of continuous surface transitions in

 This journal is © The Royal Society of Chemistry 2018

the wedge. This phenomena is conveniently referred to as complete pre-wetting, since a film of the thicker pre-wetting phase intrudes between the wedge bottom and the thin pre-wetting phase. Similar phenomena occur on steps, on patterned walls and in capillaries.[6,20] The nature of this transition and the exponents that characterise it will be considered in our final section. We note that, when the pre-wetting line is approached from above, the phenomenon of complete pre-wetting does not occur, and the crossing of the pre-wetting line results in a first-order transition from a thick to a thin layer, similar to that occurring at a planar wall.

3.2 Case $\alpha < \alpha^*$

If the tilt angle is smaller than the critical value, then the pre-filling and pre-wetting lines merge at two points (see Fig. 4c). Within the graphical construction, this simply means that the equal areas condition (pre-filling) occurs when the binding potential has coexisting minima (pre-wetting) – see Fig. 6. Using the binding potential (7), we have determined the pre-wetting line and the value of α for which the equal areas criterion also applies. The resulting curve $\tilde{\alpha}(T)$ is shown in Fig. 7. The critical value α^* simply corresponds to the maximum of this curve. For the potential (7), we have determined this as

$$\alpha^* \approx 0.10873\sqrt{\frac{B^4}{16C^3\sigma}} \qquad (8)$$

where $B^4/16C^3$ is a natural unit of energy per unit area for this potential. Using values for B and C as determined by a microscopic sharp-kink approximation,[19] we estimate that the critical value α^* is small – of the order of a few degrees.

For $\alpha > \alpha^*$, we have already noted that there are no intersections and the pre-wetting and pre-filling lines do not cross. For $\alpha < \alpha^*$, on the other hand, there are two intersections at T_1^* and T_2^* which, for very shallow wedges, occur near T_w and T_{pw}^c respectively. The function $\tilde{\alpha}(T)$ vanishes at the wetting temperature T_w and at the pre-wetting critical point for different reasons. Recall that, on approaching T_w, the thickness $\ell_\pi^{(+)}$ of the thick pre-wetting layer diverges, which means that $\tilde{\alpha}(T)$ must be very small in order to balance the areas in the graphical construction, due to the long tail in $W(\ell)$. Our numerical calculations indicate that, close to the wetting temperature, the curve behaves as $\tilde{\alpha}(T) \propto (T - T_w)^{1/2}$ with multiplicative logarithmic corrections, for the present case of dispersion-like forces. On the other hand, near the pre-wetting critical point, where $\Delta W(\ell)$ can be approximated reliably as a quartic function, a simple calculation determines that $\tilde{\alpha}(T) \approx (\ell_\pi^{(+)} - \ell_\pi^{(-)})/\xi_\parallel$. Here, as before, $\ell_\pi^{(+)}$ (thick) and $\ell_\pi^{(-)}$ (thin) are the coexisting wetting film thicknesses, while $\xi_\parallel = \sqrt{\sigma \Big/ W''\left(\ell_\pi^{(+)}\right)}$ is the correlation length along the wall. This means that the curve $\tilde{\alpha}(T)$ vanishes linearly on approaching the end of the pre-wetting line as $\tilde{\alpha}(T) \propto (T_{pw}^c - T)$.

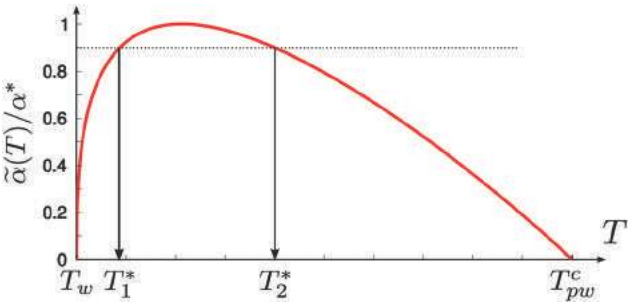

Fig. 7 The curve $\tilde{\alpha}(T)$ computed numerically for the potential (7). For a given tilt angle $\alpha < \alpha^*$, the intersection of a horizontal line with this curve determines the temperatures T_1^* and T_2^* at which the pre-wetting and pre-filling lines merge.

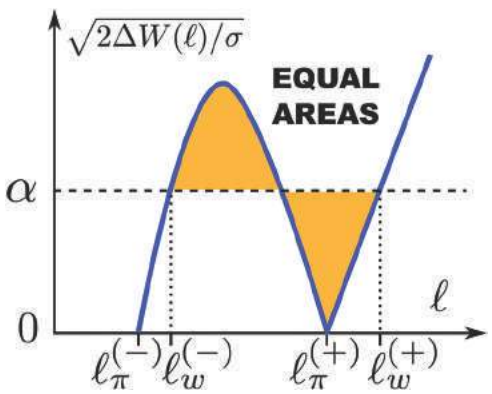

Fig. 6 Equal areas construction determining the merging of the pre-filling and pre-wetting lines (see text for details). This construction is equivalent to that determining the location of a first-order wetting transition within the Cahn theory of wetting for the case of zero surface enhancement.[8,9]

A representative phase diagram for the case $\alpha < \alpha^*$ is shown in Fig. 4(c), along with a schema for purposes of illustration. The latter shows a number of different sections and associated interfacial phase transitions. The pre-filling line consists of two sections, labelled PF1 and PF2, which meet the pre-wetting line tangentially at the two temperatures; T_1^* and T_2^*. Crossing the lines PF1 and PF2 results in a first-order pre-filling transition similar to the one described for $\alpha > \alpha^*$: the local interfacial height ℓ_w jumps, while the wetting height far from the apex remains constant. The pre-wetting line has the same location as that occurring at a flat wall $p = p_{pw}(T)$ but must be regarded as comprising three sections. On approaching the sections PW1 or PW2 (from below), a continuous complete pre-wetting transition is induced, *i.e.* the wetting films along the side walls develop a shoulder of the thicker pre-wetting film phase $\ell_\pi^{(+)}$, the length of which h grows continuously as the phase boundary is approached (similar to those in Fig. 5). This aspect of the phase diagram was not identified correctly in ref. 2. However, in the middle section of the pre-wetting line, PWM, stretching from T_1^* to T_2^*, no such complete pre-wetting occurs. Crossing this line results in a first-order phase transition in which both the mid-point height ℓ_w and wetting film height ℓ_π jump from their respective thin to thick values, and becomes identical to the usual pre-wetting transition on a planar wall as $\alpha \to 0$. In this limit, the sections PW1 and PW2 (for which the pre-wetting transition is continuous) shrink to zero. Note that crossing any of the three sections of the pre-wetting line from above, results in a first-order transition from a thick to a thin layer on the side walls, as described in the previous case ($\alpha > \alpha^*$).

The merging of the pre-filling and pre-wetting lines gives rise to two new interfacial phase transitions occurring at T_1* and T_2*. Suppose that we sit in the middle section (PWM) of the pre-wetting curve at pressure $p = p_{pw}(T)^-$. Now, while remaining on the pre-wetting line, we increase the temperature towards T_2*. Exactly at T_2*, two different interfacial profiles coexist: One for which the equilibrium position of the thin-thick shoulder on the side walls is microscopically close to the wedge mid-point, the other for which the shoulder is macroscopically far away. The same also happens as the temperature is decreased towards T_1*. In both cases, the discontinuous unbinding of the shoulder between the thin and thick pre-wetting phases is equivalent to a first-order wetting transition, but now occurring along the walls (*i.e.* in two-dimensions). These transitions correspond to the intrusion of a macroscopic layer of the thick pre-wetting film between the liquid nucleated near the wedge bottom and the thin pre-wetting film far from it, *i.e.* the discontinuous divergence of the length h. At mean-field level, these transitions must be first-order since the graphical construction for the interfacial profile is equivalent to the Cahn construction for wetting with zero surface enhancement.[8,9,21] Viewed this way, it is clear why the pre-filling lines PF1 and PF2 must meet the pre-wetting line tangentially: for the same reason that the pre-wetting line meets the bulk coexistence curve tangentially.

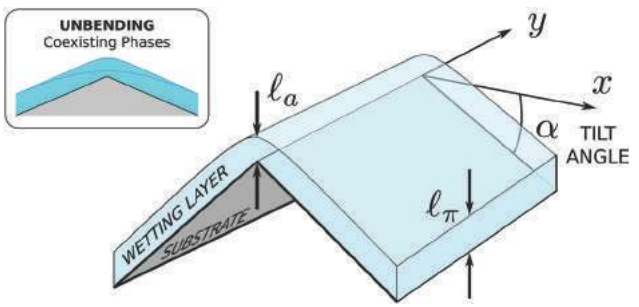

Fig. 8 Schematic illustration of an interfacial configuration near an apex showing the reduction of the local adsorption of liquid near the tip. Inset: Coexisting interfacial profiles at an unbending transition.

4 Pre-wetting and unbending near an apex tip

When the tilt angle is negative, the substrate forms the shape of an infinite apex tip rather than a wedge (see Fig. 8). Adsorption near an apex has been studied previously but the interplay with pre-wetting has not been considered.[22,23] Quite generally, an apex does not have a filling transition, but may exhibit an unbending transition between phases with thin and thicker adsorptions of liquid near the tip (see inset). This transition occurs because the thin phase reduces the liquid–gas interfacial area, while the thick phase avoids the penalty cost in the free energy arising from the repulsive barrier in the binding potential, present for substrates that exhibit first-order wetting. The unbending transition, and in particular its relation with pre-wetting, can be analysed using the simple interfacial model (2) and similar graphical approach. However, the mid-point height at an apex $\ell_a = \ell(0)$ is smaller than the planar wetting film thickness ℓ_π. This means that phase transitions now occur above the pre-wetting line (*i.e.* when the planar wetting film is the "thicker" phase). Representative graphical constructions are shown in Fig. 9. The final figure (Fig. 9c) is an equal areas condition which determines a curve $\bar{\alpha}(T)$ (see Fig. 10), analogous to the earlier $\tilde{\alpha}(T)$. Using this approach, we can see that the unbending transition necessarily occurs above the pre-wetting line, and that the line of unbending transitions in the $(T,\Delta p)$ plane always ends at a critical point lying on the upper pre-wetting spinodal line. This is analogous to the location of the pre-filling critical point, which lies on the lower pre-wetting spinodal for the wedge.

The location of the unbending line in relation to pre-wetting is determined by the angle α, defined by $z_w = -|x|\tan\alpha$ (so that $\alpha > 0$). There are three scenarios as shown in Fig. 11. For large values of $\alpha > \alpha^{\dagger\dagger}$, no unbending transition exists. The critical value is determined by $\alpha^{\dagger\dagger} = \sqrt{2\Delta W/\sigma}$, where ΔW is evaluated at its inflexion point and at the crossing of the upper spinodal and the liquid–gas coexistence line. In turn, for sufficiently small values $\alpha < \alpha^{\dagger}$, the unbending line meets the pre-wetting line tangentially at a temperature T_3* determined by the

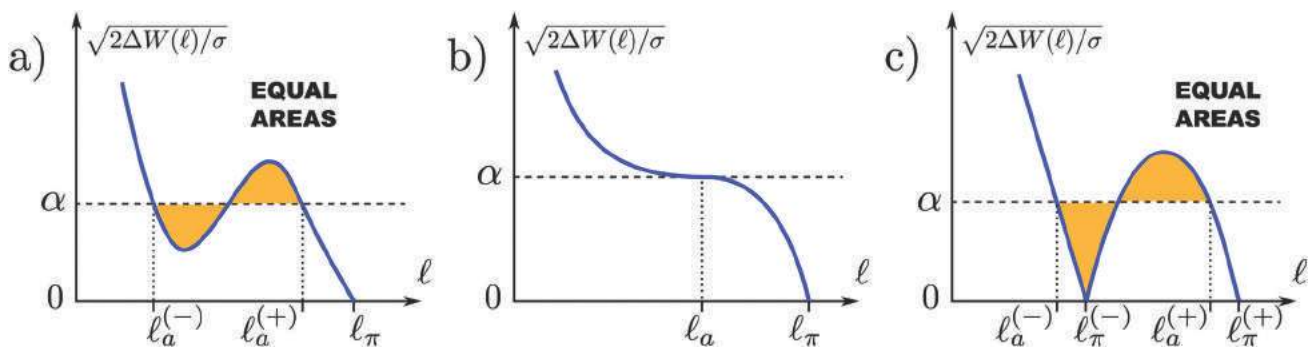

Fig. 9 Representative graphical constructions determining the surface phase diagram for fluid adsorption near an apex tip: (a) equal areas construction for an unbending transition showing coexisting profiles with different thin ($\ell_a^{(-)}$) and thick ($\ell_a^{(+)}$) mid-point heights, (b) an unbending critical point occurring off bulk liquid–gas coexistence, (c) simultaneous occurrence of unbending and pre-wetting. Moving along the pre-wetting line, this latter construction is used in the determination of $\bar{\alpha}(T)$.

This journal is © The Royal Society of Chemistry 2018

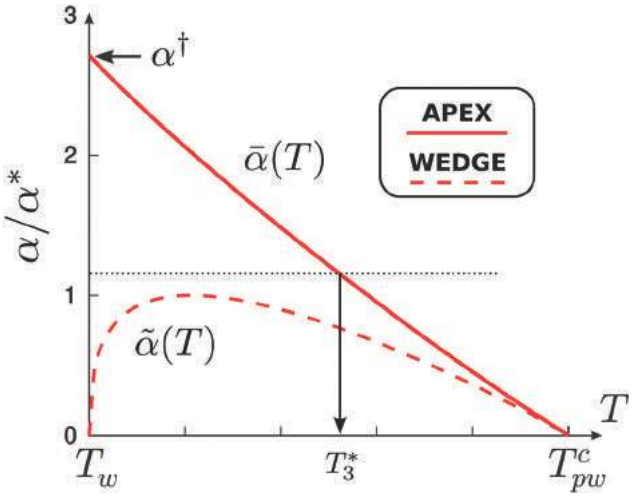

Fig. 10 The curve $\bar{\alpha}(T)$ computed numerically for the potential (7). For a given tilt angle $\alpha < \alpha^\dagger$, the intersection of a horizontal line with this curve determines the temperatures T_3* at which the pre-wetting and unbending lines merge. The curve $\tilde{\alpha}(T)$ for a wedge is shown for comparison.

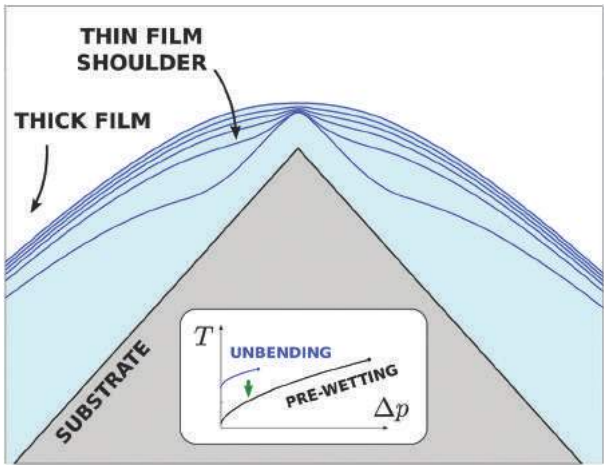

Fig. 12 Interfacial profiles in the approach to a complete pre-wetting transition as the pre-wetting line is approached from above (green arrow in inset). On approaching the pre-wetting line, the profile develops a large shoulder of the thinner pre-wetting film which intrudes between the apex tip and the thick pre-wetting layer. The length of this complete pre-wetting layer diverges continuously as the pre-wetting line is approached. See Fig. 5 for comparison with the analogous transition occurring for the wedge.

intersection of α with the curve $\bar{\alpha}(T)$. Note that $\alpha^\dagger \equiv \bar{\alpha}(0) > 0$, since the thin pre-wetting film thickness does not diverge at T_w. For intermediate values $\alpha^\dagger < \alpha < \alpha^{\dagger\dagger}$, the pre-wetting and unbending lines are separate. For the potential (7), we find that $\alpha^{\dagger\dagger}/\alpha^* \approx 4.2242$ and $\alpha^\dagger/\alpha^* \approx 2.7127$ where, recall, α^* is given by (8) and is itself estimated to be a few degrees.

Similar to the wedge geometry, the apex induces a complete pre-wetting transition along the side walls, but now occurring when the pre-wetting line is approached from above (*i.e.* $p \to p_{pw}(T)^+$). For $\alpha > \alpha^\dagger$, this occurs along the whole pre-wetting line while. For $\alpha < \alpha^\dagger$, it occurs only for $T > T_3$*. In each case, on approaching the pre-wetting line from above, a macroscopic layer of the thinner pre-wetting phase intrudes between the apex tip and the thick pre-wetting film (*i.e.* the opposite of the complete pre-wetting transition for the wedge). Representative interfacial profiles are shown in Fig. 12. Finally, the merging of the unbending and pre-wetting lines at T_3* corresponds to a 2D wetting transition occurring at the side walls (which is first-order in the present mean-field approximation), similar to the transitions ocurring at T_1* and T_2* in the wedge. In the limit $\alpha \to 0$, T_3* tends to T_{pc}^c, so that one recovers the usual line of first-order pre-wetting transition.

5 Fluctuation effects and critical singularities

To finish our article, we discuss how the above mean-field considerations are modified when fluctuation effects are included. As noted in previous work, since the wedge geometry is effectively one dimensional, the pre-filling transition must be rounded by fluctuations so that the adsorption increases sharply near the pre-filling line rather than jumping discontinuously.[2] These are shown as blurred lines in the schematic phase diagram of Fig. 13.

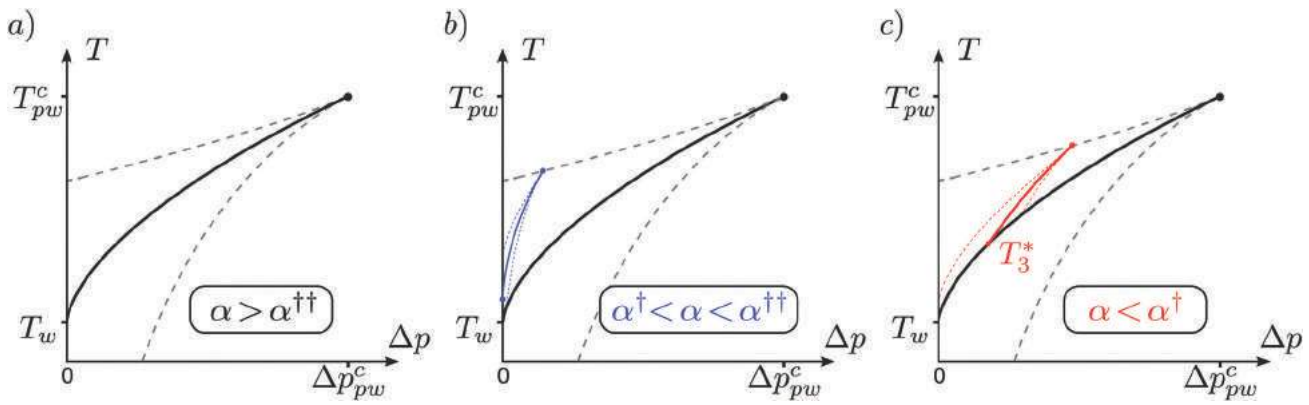

Fig. 11 Surface phase diagram for first-order wetting near an apex tip computed numerically using the binding potential (7): (a) $\alpha > \alpha^{\dagger\dagger}$, for which no unbending line exists, (b) $\alpha^\dagger < \alpha < \alpha^{\dagger\dagger}$, for which the unbending (blue) and pre-wetting (black) lines are separate, and (c) $\alpha < \alpha^\dagger$, where the unbending (red) and pre-wetting (black) lines merge tangentially at T_3*. The dashed lines represent the corresponding spinodals.

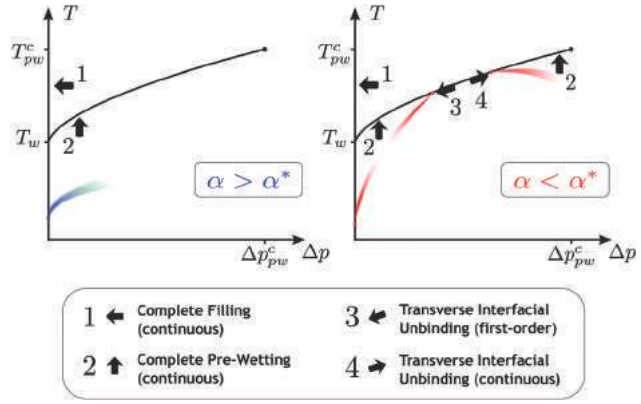

Fig. 13 Schematic phase diagrams for first-order wedge filling, beyond mean-field for $\alpha > \alpha^*$ and $\alpha < \alpha^*$. The blurred lines represent the locations of sharply rounded, pseudo first-order pre-filling transitions with respect to the pre-wetting line (black curve). The arrows indicate the paths along which different interfacial unbinding transitions may occur: The meniscus unbinds at complete filling (path 1), while the thin-thick interface at the side walls unbinds at complete pre-wetting (path 2). The paths 3 and 4 along the pre-wetting line approaching T_1^* and T_2^*, respectively, represent transverse interfacial unbinding transitions.

Standard finite-size scaling arguments[24] suggest that the rounding of the transition occurs over a narrow range of pressures or temperatures of order $\exp(-\beta\sigma\ell_w^{(+)2})$, where $\ell_w^{(+)}$ is the height of the "thicker" pre-filling layer. This estimate is based on the Boltzmann weight of forming a domain wall between the microscopically thin and mesoscopically thick pre-filling phases. Near bulk coexistence, we anticipate that $\ell_w \propto \Delta p^{-1}$, so that the rounding of the transition is negligible. Indeed, the first-order filling transition itself still persists at the filling temperature T_f. However, there is certainly no pre-filling critical point beyond mean-field level.

The phase transitions that remain when fluctuation effects are included are all different examples of interfacial unbinding. There are four types:

(1) Complete filling (paths 1). The complete filling transition refers to the continuous divergence of the interfacial height ℓ_w on approaching bulk coexistence along an isotherm for temperatures $T > T_f$. This transition can be understood using purely macroscopic arguments since, close to coexistence, the equilibrium interfacial shape must correspond to a meniscus of near circular cross-section with Laplace radius $R = \sigma/\Delta p$ which meets the walls at the contact angle.[25,26] Elementary calculation then determines that, on approaching bulk coexistence, the interfacial height diverges as

$$\ell_w = \frac{\sigma(\sec\alpha\cos\theta - 1)}{\Delta p} + \cdots \qquad (9)$$

Indeed, the small angle version of this follows immediately from solution of the mean-field eqn (6). This macroscopic result is not influenced by interfacial wandering even in two dimensions, where fluctuation effects are strongest.[27] Notice that the nature of complete filling is slightly different in the regions $T_f < T < T_w$ and $T > T_w$. Above the wetting temperature, where we must set $\theta = 0$ in (9), the higher-order terms are also singular arising from the divergence of the wetting film height $\ell_\pi \propto \Delta p^{-\beta_s^{co}}$, with $\beta_s^{co} = 1/3$ for systems with long-ranged dispersion forces.[28]

(2) Complete pre-wetting (paths 2). As discussed earlier, complete pre-wetting refers to the continuous growth in the equilibrium length h of a shoulder of the thick pre-wetting layer at each wall, as the pre-wetting line is approached from below. For $\alpha > \alpha^*$, this happens along the entire pre-wetting line, while for $\alpha < \alpha^*$ it occurs along the sections PW1 and PW2 only. For fixed temperature T, let us denote $\delta p = p_{pw}(T) - p$ as the deviation from the pressure at pre-wetting. We wish now to determine how the pre-wetting film thickness h grows as $\delta p \to 0$. It is straightforward to show from integration of the profile eqn (4) that, according to the simple interfacial model (2), the equilibrium film thickness along the side walls diverges as $h \approx -\xi_\parallel^{(+)} \ln \delta p$. Here, $\xi_\parallel^{(+)} = \sqrt{\sigma \big/ W''\left(\ell_\pi^{(+)}\right)}$ is the parallel correlation length defined for the thicker pre-wetting film on a planar wall. This result emerges for any binding potential $W(\ell)$, with a double-well structure used to model pre-wetting. However, this quantitative prediction is not correct for systems with long-ranged forces, since the local model (2) fails to account for the influence of intermolecular forces along the wall.

To handle these correctly, we resort to another interfacial model designed specifically to model fluctuation effects and interactions near the complete pre-wetting transition. This second interfacial model takes the form

$$F[h] = \int \mathrm{d}y \left(\frac{\tilde{\tau}}{2} \left(\frac{\mathrm{d}h}{\mathrm{d}y} \right)^2 + V(h) \right) \qquad (10)$$

where $h(y)$ is now the local distance of the thick/thin interface measured from the wedge bottom at position y along it (see Fig. 14). Here, $\tilde{\tau}$ is the line tension associated with the interface between pre-wetting films of heights $\ell_\pi^{(-)}$ and $\ell_\pi^{(+)}$, which controls the free-energy cost of undulations in the position of the thin/thick interface. A mean-field expression for this can be derived from the capillary-wave model (2) yielding

$$\tilde{\tau} = \sigma \int_{\ell_\pi^{(-)}}^{\ell_\pi^{(+)}} \mathrm{d}\ell \left(\sqrt{\frac{2\Delta W(\ell)}{\sigma}} - \alpha \right) \qquad (11)$$

This expression is consistent with the two general expectations: (a) that the line tension vanishes at the pre-wetting critical point, and (b) that it is very large near the wetting temperature, where it is well approximated by $\tilde{\tau} \approx \ell_\pi^{(+)}\sigma$. Recall that the film height of the thicker pre-wetting layer $\ell_\pi^{(+)}$, and hence $\tilde{\tau}$, diverges as we approach T_w along the pre-wetting curve.

The potential $V(h)$ accounts for the direct interaction of the thick/thin interface with the wedge bottom arising from all the intermolecular forces in the system. For systems with short-ranged wall–fluid and fluid–fluid forces (*e.g.* finite-range or exponentially decaying), this potential can be derived from the underlying Capillary-Wave model (2) using standard techniques, and takes the form[29]

$$V_{SR}(h) = \delta p\, \Delta\ell\, h + C' \mathrm{e}^{-h/\xi_\parallel^{(+)}} + \cdots \qquad (12)$$

This journal is © The Royal Society of Chemistry 2018

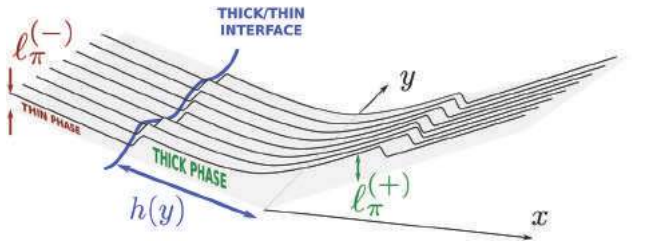

Fig. 14 Schematic illustration of the interfacial wandering of the thin-thick interface along the side walls of a wedge, together with the collective coordinate $h(y)$ appearing in the effective Hamiltonian (10).

where $C' > 0$ is an unimportant constant and $\Delta\ell = \ell_\pi^{(+)} - \ell_\pi^{(-)}$ is simply the difference between the two pre-wetting film heights. The first term of $V_{\rm SR}(h)$ is the thermodynamic cost of having a large film of the metastable thicker pre-wetting layer near the wedge bottom. The second term is the repulsion which must be mediated by the parallel correlation length $\xi_\parallel^{(+)}$, which controls the decay of order in the thick film region. Minimization of $V_{\rm SR}(h)$ then recovers the mean-field result $h \propto -\xi_\parallel^{(+)} \ln \delta p$, quoted above. This approach clearly brings out the analogy with (two dimensional) complete wetting transitions. The expression (10) is equivalent to the effective Hamiltonian for 2D wetting, which can be studied exactly using transfer matrix techniques. This means that, beyond mean-field, fluctuations in the edge of the unbinding thin/thick interface alter this logarithmic divergence to $h \propto \delta p^{-1/3}$.[30]

The analogy with 2D complete wetting persists for systems with long-ranged (algebraically decaying) fluid–fluid and wall–fluid forces, but here we must work a little harder to construct the potential $V_{\rm LR}(h)$. The reason for this is that the form of $V_{\rm LR}(h)$ cannot be determined from the shallow wedge model (2) since this does not account for long-ranged interactions along the wall. However, we can construct $V_{\rm LR}(h)$ by appealing to more microscopic models of fluid adsorption in a wedge based on Density Functional Theory. The task of determining the potential $V_{\rm LR}(h)$ for the complete pre-wetting transition is made easier because its form is dominated by the wall–fluid forces. The reason for this is that the liquid layer adsorbed at the side walls is only pseudo two-dimensional while the wall has a full 3D volume. This means that the long-ranged decay of the potential $V_{\rm LR}(h)$ is determined fully by the external potential arising from the wall–fluid interaction. For systems with dispersion forces, this is known analytically[5] and leads to

$$V_{\rm LR}(h) = \delta p \Delta\ell h + \frac{A_{\rm wf}\Delta\ell \tan\alpha\left(3+\tan^2\alpha\right)}{8} h^{-2} + \cdots \qquad (13)$$

and recall that $A_{\rm wf} > 0$ is the wall–fluid contribution to the Hamaker constant. Minimization of this potential determines the mean-field position of the thin-thick interface and shows that, in the presence of long-ranged forces, it diverges as $h \approx \delta p^{-1/3}$ on approaching the pre-wetting line. This result is only weakly affected by fluctuation effects, which only alter the amplitude of the divergence but not the value of the critical exponent.[30]

(3) Transverse interfacial unbinding transitions at T_1^* and T_2^* (paths 3 and 4). Finally, we turn our attention to the two transitions occurring as the temperature is increased towards T_2^* or decreased towards T_1^* while remaining on the pre-wetting coexistence curve ($\delta p = 0^-$). Recall that these transitions correspond to the unbinding of the thin–thick interface, and are analogous to 2D wetting transitions. At mean-field level, these transitions are certainly first-order so that the value of h jumps discontinuously from a microscopic to macroscopic value. This means that the appropriate potential $V_{\rm SR}(h)$ or $V_{\rm LR}(h)$ must have a short-ranged attraction and also a potential barrier – directly analogous to the form of the potential $W(\ell)$ modelling 3D wetting transitions. However, the character of these transitions is now strongly influenced by interfacial fluctuations arising from the wandering of the thin–thick interface. For example, in systems with short-ranged forces the transitions occurring at T_1^* and T_2^* must now belong to the universality class of 2D short-ranged critical wetting transitions[31] (the strong-fluctuation regime in the general classification of wetting transitions[32]). That is, we expect that the distance of the thin–thick interface from the wedge bottom diverges continuously as $h \approx (T - T_1^*)^{-1}$ and $h \approx (T_2^* - T)^{-1}$, as T is decreased and increased towards T_1^* and T_2^*, respectively, at $\delta p = 0^-$. However, the size of the asymptotic critical regime, where such universal critical behaviour can be observed, is extremely small due to the tunnelling required to penetrate through the potential barrier. Thus, we anticipate that the transitions occurring at both T_1^* and T_2^* would be examples of apparent first-order wetting similar to that discussed recently in the literature.[33,34]

For systems with long-ranged forces, something even more subtle occurs. In this case, a short-ranged attractive term in $V_{\rm LR}(h)$ competes against the long-ranged repulsion described by the second-term in (13). The inverse square decay ($\propto h^{-2}$) is a marginal interaction for 2D wetting, implying that the two transitions occurring at T_1^* and T_2^* must belong to the intermediate-fluctuation regime of critical wetting.[10] This regime further sub-divides into three sub-regimes, depending on the value of the coefficient of the inverse square decay and the line tension $\tilde\tau$. If $A_{\rm wf}\tilde\tau\Delta\ell\tan\alpha\left(1+\frac{1}{3}\tan^2\alpha\right)\Big/(k_{\rm B}T)^2 > 1$ the thin–thick unbinding transition remains strictly first-order, but is characterised by strongly non-Gaussian fluctuations. In general, this will be the case for the unbinding transition occurring at T_1^*, since the transition temperature occurs close to $T_{\rm w}$ – for which both $\tilde\tau$ and $\Delta\ell$ are macroscopically large. Thus, the transition occurring at T_1^* will be first-order, similar to the predictions of mean-field theory.

However, we can expect more dramatic behaviour for the transition occurring at T_2^*, since this temperature is, in general, close to the pre-wetting critical point, where $\tilde\tau$ and $\Delta\ell$ are small. Thus, we can anticipate that $A_{\rm wf}\beta^2\tilde\tau\Delta\ell\tan\alpha\left(1+\frac{1}{3}\tan^2\alpha\right) < 1$. In this case, the transition belongs to sub-regime B of the intermediate fluctuation regime, corresponding to continuous wetting characterised by non-universal critical exponents.[10] Thus, for the transition occurring at T_2^*, we expect that the distance of the thin-thick interface from the wedge bottom diverges

continuously as $h \approx (T_2^* - T)^{-\beta_s}$ with an angle-dependent critical exponent

$$\beta_s = \frac{1}{\sqrt{1 + a\tan\alpha(3 + \tan^2\alpha)}} \quad (14)$$

where $a = A_{wf}\tilde{\tau}\Delta\ell/(k_B T)^2$ is a temperature dependent, non-universal constant.

Fluctuation effects influence the phase transitions occurring at the apex in a similar manner. The unbending transition is always rounded, even more so than the pre-filling transition, since the difference in the coexisting adsorptions near the apex tip is microscopic. The two phase transitions which are left are complete pre-wetting (that occurs all along the pre-wetting line for $\alpha > \alpha^\dagger$ and for $T > T_3^*$ and $\alpha < \alpha^\dagger$) and the unbinding of the thick–thin interface along the side walls as $T \to T_3^*$ at $\delta p = 0^+$. The fluctuation effects occurring at these transitions are the same as those described above for the wedge. In particular, for systems with dispersion forces, the unbinding transition occurring at T_3^* will belong to fluctuation regime C (first-order) if $A_{wf}\beta^2\tilde{\tau}\Delta\ell\tan\alpha\left(1 + \frac{1}{3}\tan^2\alpha\right) > 1$, or fluctuation regime B (continuous with non-universal exponents) otherwise.

6 Discussion

In this paper, we have used simple interfacial Hamiltonian models to show that rather rich phase diagrams, showing different types of interfacial unbinding transitions, may occur for fluids adsorbed near wedges and apexes, when the wall–fluid interface exhibits first-order wetting. These phase diagrams are considerably more involved than those predicted for systems with critical wetting due to the interplay of pre-wetting and pre-filling transitions (or unbending, in the case the apex).[2,3] The possible merging of the pre-filling and pre-wetting lines for shallow wedges had been noted previously. However, the nature of the associated interfacial unbinding transitions occurring along the side walls had not been properly understood. Our predictions for the divergence in the adsorption characterising complete pre-wetting can be tested in more microscopic Density Functional models similar to recent studies of fluids in capped capillaries.[20] This would also test the semi-quantitative prediction of the present study that the merging of the pre-filling and pre-wetting lines occurs when the tilt angle is less than a few degrees, something our simple interfacial model cannot predict with greater accuracy. The most subtle aspect of our study concerns the fluctuation-induced angle dependence of non-universal critical exponents characterising the phase transition at T_2^* for systems with long-ranged dispersion forces. While the experimental observation of such non-universality is extremely challenging, it means that, at least in principle, fluctuation effects predicted for the highly exotic intermediate fluctuation regime of 2D wetting do occur in physically accessible systems. More generally, we hope that the insights gained into the richness of the phase diagrams for wedges and apexes can help us understand what happens when such geometries are used as the building blocks for more complicated nano-patterned substrates.

Conflicts of interest

There are no conflicts to declare.

Acknowledgements

This work was partly funded by the EPSRC UK grant EP/L020564/1, ''Multiscale Analysis of Complex Interfacial Phenomena'' and a studentship (JP). C. R. also acknowledges the support of the grant FIS2015-66523-P (MINECO/FEDER, UE).

Notes and references

1 K. Binder, *Annu. Rev. Mater. Res.*, 2008, **38**, 123.
2 K. Rejmer, S. Dietrich and M. Napiórkowski, *Phys. Rev. E: Stat., Nonlinear, Soft Matter Phys.*, 1999, **60**, 4027.
3 A. O. Parry, C. Rascón and A. J. Wood, *Phys. Rev. Lett.*, 2000, **85**, 345.
4 A. Malijevský and A. O. Parry, *Phys. Rev. Lett.*, 2013, **110**, 166101.
5 A. Malijevský and A. O. Parry, *Phys. Rev. E: Stat., Nonlinear, Soft Matter Phys.*, 2015, **91**, 052401.
6 W. F. Saam, *J. Low Temp. Phys.*, 2009, **157**, 77.
7 P. Yatsyshin, A. O. Parry and S. Kalliadasis, *J. Phys.: Condens. Matter*, 2016, **28**, 275001.
8 J. W. Cahn, *J. Chem. Phys.*, 1977, **66**, 3667.
9 D. E. Sullivan and M. M. Telo da Gama, in *Fluid Interfacial Phenomena*, ed. C. A. Croxton, John Wiley and Sons Ltd, 1986, ch. 2.
10 R. Lipowsky and T. M. Nieuwenhuizen, *J. Phys. A: Math. Gen.*, 1988, **21**, L89.
11 C. Rascón, A. O. Parry and A. Sartori, *Phys. Rev. E: Stat. Phys., Plasmas, Fluids, Relat. Interdiscip. Top.*, 1999, **59**, 5697.
12 D. E. Sullivan, *Phys. Rev. B: Condens. Matter Mater. Phys.*, 1979, **20**, 3991.
13 S. Dietrich, in *Phase Transitions and Critical Phenomena*, ed. C. Domb and J. Lebowitz, Academic Press Limited, 1988, vol. 12.
14 M. Schick, in *Liquids at interfaces*, ed. J. Charvolin, J. F. Joanny and J. Zinn-Justin, Elsevier, 1990.
15 D. Bonn, J. Eggers, J. O. Indekeu, J. Meunier and E. Rolley, *Rev. Mod. Phys.*, 2009, **81**, 739.
16 P. Concus and R. Finn, *Proc. Natl. Acad. Sci. U. S. A.*, 1969, **63**, 292.
17 Y. Pomeau, *J. Colloid Interface Sci.*, 1986, **113**, 5.
18 E. H. Hauge, *Phys. Rev. A: At., Mol., Opt. Phys.*, 1992, **46**, 4994.
19 S. Dietrich and M. Napiórkowski, *Phys. Rev. A: At., Mol., Opt. Phys.*, 1991, **43**, 1861.
20 P. Yatsyshin, N. Savva and S. Kalliadasis, *Phys. Rev. E: Stat., Nonlinear, Soft Matter Phys.*, 2013, **87**, 020402(R).
21 H. Nakanishi and M. E. Fisher, *Phys. Rev. Lett.*, 1982, **49**, 1565.

 This journal is © The Royal Society of Chemistry 2018

22 A. O. Parry, M. J. Greenall and J. M. Romero-Enrique, *Phys. Rev. Lett.*, 2003, **90**, 46101.
23 A. Malijevský, *J. Phys.: Condens. Matter*, 2014, **26**, 315002.
24 V. Privman and M. E. Fisher, *J. Stat. Phys.*, 1983, **33**, 385.
25 C. Rascón and A. O. Parry, *J. Chem. Phys.*, 2000, **112**, 5175.
26 C. Rascón and A. O. Parry, *Nature*, 2000, **407**, 986.
27 A. O. Parry, C. Rascón and A. J. Wood, *Phys. Rev. Lett.*, 1999, **83**, 5535.
28 C. Rascón and A. O. Parry, *Phys. Rev. Lett.*, 2005, **94**, 096103.
29 A. O. Parry, C. Rascón, E. A. G. Jamie and D. G. A. L. Aarts, *Phys. Rev. Lett.*, 2012, **108**, 246101.
30 R. Lipowsky, *Phys. Rev. B: Condens. Matter Mater. Phys.*, 1985, **32**, 1731.
31 D. B. Abraham, *Phys. Rev. Lett.*, 1980, **44**, 1165.
32 R. Lipowsky and M. E. Fisher, *Phys. Rev. B: Condens. Matter Mater. Phys.*, 1987, **36**, 2126.
33 X. T. Wu, D. B. Abraham and J. O. Indekeu, *Phys. Rev. Lett.*, 2016, **116**, 046101.
34 A. O. Parry and A. Malijevský, *Phys. Rev. E*, 2016, **93**, 062802.

This journal is © The Royal Society of Chemistry 2018